Nuclear Instruments and Methods in Physics Research B 269 (2011) 1316–1320

Contents lists available at ScienceDirect

Nuclear Instruments and Methods in Physics Research B

journal homepage: www.elsevier.com/locate/nimb

Sputtering of lunar regolith simulant by protons and singly and multicharged Ar ions at solar wind energies

F.W. Meyer [a,*], P.R. Harris [a], C.N. Taylor [a,1], H.M. Meyer III [b], A.F. Barghouty [c], J.H. Adams [c]

[a] Physics Division, Oak Ridge National Laboratory, P.O. Box 2008, Oak Ridge, TN 37831, United States
[b] MST Division, Oak Ridge National Laboratory, P.O. Box 2008, Oak Ridge, TN 37831, United States
[c] NASA-Marshall Space Flight Center, Huntsville, AL 35812, United States

ARTICLE INFO

Article history:
Received 3 November 2010
Received in revised form 29 November 2010
Available online 5 December 2010

Keywords:
Solar wind
Sputtering
Lunar regolith
Ion-surface interactions

ABSTRACT

We report preliminary results on sputtering of a lunar regolith simulant at room temperature by singly and multiply charged solar wind ions using quadrupole and time-of-flight (TOF) mass spectrometry approaches. Sputtering of the lunar regolith by solar-wind heavy ions may be an important particle source that contributes to the composition of the lunar exosphere, and is a possible mechanism for lunar surface ageing and compositional modification. The measurements were performed in order to assess the relative sputtering efficiency of protons, which are the dominant constituent of the solar wind, and less abundant heavier multicharged solar wind constituents, which have higher physical sputtering yields than same-velocity protons, and whose sputtering yields may be further enhanced due to potential sputtering. Two different target preparation approaches using JSC-1A AGGL lunar regolith simulant are described and compared using SEM and XPS surface analysis.

© 2010 Published by Elsevier B.V.

1. Introduction

The sputtering yields for lunar regolith impacted by the various solar wind constituent ions are important parameters in estimates of solar wind induced compositional changes in the lunar surface and its erosion rate. In addition, knowledge of such yields helps determine the contribution of the solar wind–lunar surface interaction to the lunar exosphere and may permit assessment of the possible role of solar wind sputtering in the accumulation of hydrogen and water on the moon's surface.

Due to their low mass in comparison to the atomic constituents of lunar regolith, the physical sputtering yields for protons, the dominant solar wind constituent, incident at solar wind velocities are small (significantly less than unity [1]). The minority constituents of the solar wind have significantly higher physical sputtering yields at solar wind velocities because of their larger atomic mass [1]. Their sputtering yields may be further enhanced by potential sputtering processes [2,3], since the minority constituents are all multiply charged, and since the lunar regolith consists mainly of insulating metal oxides [4].

Typical solar wind particle fluxes are of the order of 10^{12} particles/m^2 s. The proton flux is about 93% of this total charged-particle flux. The remaining ≈7% is distributed among the major multicharged solar-wind heavy ions (SWHI) according to Table 1 [5,6]. Typical solar wind velocities fall in the range 350–1200 eV/amu.

In this contribution, we present preliminary results comparing mass resolved sputtering in the range 2–20 amu by 375 eV/amu protons and same-velocity Ar^{+}, Ar^{6+}, and Ar^{9+} ions. The Ar^{6+} and Ar^{9+} ions were used as proxies for solar wind multicharged ions having neutralization potential energies in the range 300–1000 eV. Comparison of relative sputtering yields for Ar^{+}, Ar^{6+}, and Ar^{9+} incident ions provides initial insights into potential sputtering enhancements that could be expected for solar wind multicharged ions having similar neutralization potential energies [1]. Weighted by their respective abundances in the solar wind, such relative measurements are a first step in assessing the role of minority multicharged constituents of the solar wind in lunar regolith sputtering.

2. Experimental approach

The typical ranges of SWHI in solids at solar wind velocities are in the 10 nm range. This range is comparable to the thickness of the amorphous melt layer, called "rim", surrounding individual lunar soil grains. The lunar regolith simulant JSC-1A AGGL [7] has such "rim" features, and was used for the present measurements. In order to permit vertical orientation of our targets, the initial samples were prepared by pressing the simulant powder into a metallic holder, which resulted in a density increase of 38%

* Corresponding author.
E-mail address: meyerfw@ornl.gov (F.W. Meyer).
[1] HERE participant from the Purdue University School of Nuclear Engineering.

0168-583X/$ - see front matter © 2010 Published by Elsevier B.V.
doi:10.1016/j.nimb.2010.11.091

Table 1
Nominal number distribution of the major solar-wind heavy ions (SWHI) relative to solar-wind protons along with observed charge states of the ion (abundances are taken from [5] while charge states are from [6]).

SWHI	He	C	N	O	Ne	Mg	Si	S	Fe
Relative abundance	7×10^{-2}	5×10^{-4}	5×10^{-5}	7×10^{-4}	6×10^{-5}	1×10^{-4}	1×10^{-4}	3×10^{-5}	8×10^{-5}
Charge state	2+	4+–6+	5+–7+	6+–8+	7+–9+	7+–10+	6+–12+	6+–11+	7+–14+

compared to loose powder, sufficient to form a cohesive aggregate. Comparison of X-ray photoelectron spectroscopy (XPS) analyses of the pressed samples and the original unpressed simulant material indicated no major change in chemical composition after pressing. We also tried an alternative sample preparation method which involved gently pressing the simulant powder, presifted to a 180 μm maximum grain size, onto UHV compatible carbon tape. Figs. 1a and 1b compare scanning electron micrographs (SEMs) of targets prepared using the two different methods, while Tables 2a and 2b compare the chemical composition of the two targets as determined by XPS. In anticipation of the higher adventitious C abundance using the second target preparation method, evident in Table 2b, our second target included a bare C tape section onto which beam could be directed to determine possible matrix or background effects due to beam interactions directly with the C tape. This second target preparation method was used in recent TOF measurements of regolith simulant sputtering, results of which, however, are still undergoing analysis and are not presented here.

The sputtering measurements for these samples were carried out at the floating surface-scattering end station of the ORNL Multicharged Ion Research Facility (MIRF) [8]. This apparatus has been used previously to study chemical sputtering of graphite [9], multicharged ion induced secondary electron emission [10], projectile neutralization [11], secondary ion production using TOF SIMS [12], and other interactions of singly and multiply charged atomic and molecular ions with metal, semiconductor, and insulator surfaces.

The MIRF CAPRICE electron cyclotron resonance (ECR) ion source [13] was used for producing the investigated H^+ and Ar^{q+} beams at 10–15 kV source potentials. Beam deceleration optics at the entrance to the floating surface scattering chamber were used to deliver all investigated beams at the same final impact velocity of ~375 eV/amu. The incident ion intensity was determined from the direct current reading on the sample, which could be biased at +28 V for secondary electron suppression. By comparing target

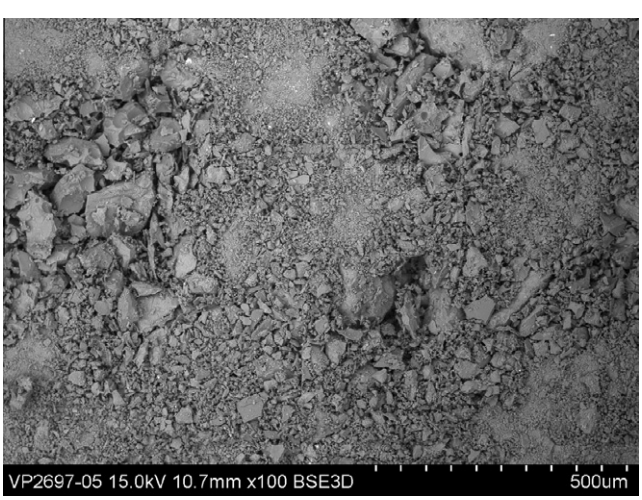

Fig. 1a. SEM of JSC-1A AGGL simulant powder pressed into a stainless steel cup to 62% of its initial uncompacted volume.

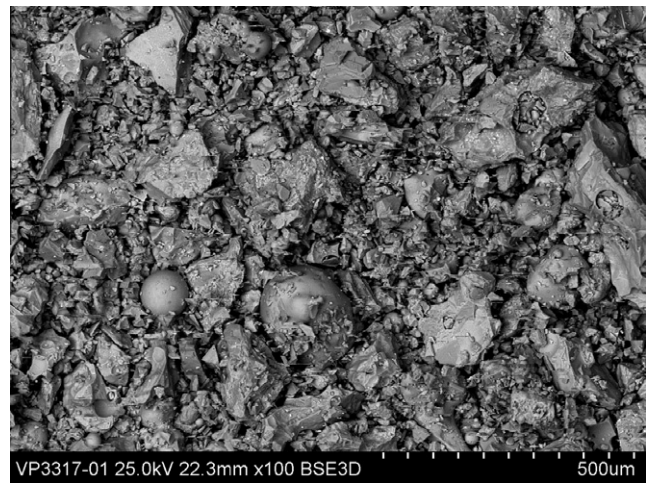

Fig. 1b. SEM of JSC-1A AGGL simulant deposited with only mild pressure onto C tape.

Table 2a
XPS analysis of four spots of pressed JSC-1A AGGL sample surface composition (atomic %).

C	O	Si	Al	Fe	Ca	Mg	Ti	Na	P	K	Cr	F
2.7	55.5	19.6	8.4	1.3	4.2	3.6	0.4	3.4	0.4	0.3	0.1	0.2
1.8	55.9	19.4	8.6	1.5	4.4	3.9	0.4	3.3	0.4	0.3	0.1	0.1
2.5	55.9	19.6	8.4	1.3	4.3	3.6	0.4	3.4	0.3	0.3	0.1	0.1
2.4	55.1	19.4	8.1	1.5	4.4	4.6	0.4	3.3	0.3	0.2	0.1	0.2
Average												
2.3	55.6	19.5	8.4	1.4	4.3	3.9	0.4	3.3	0.3	0.3	0.1	0.1

Table 2b
XPS analysis of three spots of JCS-1A AGGL sample deposited on C-tape surface composition (atomic %).

C	O	Si	Al	Fe	Ca	Mg	Ti	Na	P	K	Cr	F
16.6	49.2	17.8	6.4	1.4	2.9	1.5	0.5	2.5	0.5	0.3	0.1	0.5
15.0	50.0	18.0	6.4	1.4	2.9	1.8	0.4	2.6	0.7	0.3	0.1	0.4
14.7	50.8	17.4	6.3	1.6	3.1	1.9	0.4	2.5	0.4	0.2	0.1	0.4
Average												
15.4	50.0	17.8	6.4	1.5	3.0	1.7	0.4	2.6	0.5	0.3	0.1	0.4

current readings with the sample grounded and biased at +28 V, estimates of the secondary electron coefficients for the investigated beams incident on lunar regolith simulant could be obtained. Typically, the secondary electron emission coefficients γ for impact on the simulant target were found to be $\ll 1$. This observation was used to verify proper placement of the beam on the simulant target. When the sample was displaced to cause part of the beam to be intercepted by the edge of the stainless steel cup, the apparent γ increased significantly, consistent with the higher γs found for metal surfaces at this energy.

The floating surface-scattering end station consists of an ultra-high vacuum chamber with base pressures in the 10^{-8} Pa range, into which decelerated ion beams from the ECR ion source can be directed. The lunar regolith simulant was mounted on a sample

holder with x–y–z translation. The holder was equipped with an e-beam heater that was used to bake the sample at ~150°C to eliminate any water that had accumulated in the simulant powder during extended storage and exposure at ambient pressure and humidity. The target temperature could be monitored using a calibrated infrared (IR) thermal monitor or a chromel–alumel thermocouple. In addition the chamber was equipped with an Ar sputter gun for surface preparation and cleaning.

A sensitive quadrupole mass spectrometer was installed in the scattering chamber as shown in Fig. 2. A grounded baffle between the front end of the QMS and the target sample prevented field penetration from the QMS ionizer section into the region traversed by the incident ion beam. This baffle also blocked the line-of-sight path between the sample and the analyzer, along which projectiles backscattered from the sample could enter and cause unwanted background contributions to the measured mass spectra. A Macintosh-based data acquisition system was used to measure mass distributions at fixed intervals in time, or alternatively, to follow the intensity of selected mass peaks vs. beam exposure time, i.e. beam fluence. The evolution of peak intensities were measured vs. accumulated beam fluence to monitor changes in yields of individual species, such as oxygen, which could signal preferential depletion of selected elements in the near-surface region. The evolution of lunar dust simulant sputtering products were determined by taking differences between a pre-irradiation mass spectrum and ones acquired during irradiation at progressively larger accumulated ion beam target doses.

Sputtering measurements using the QMS approach are subject to wall collision effects [14], complicating the determination of absolute sputtering yields. In the present work, we measured sputtered particle mass distributions which were normalized by the measured particle currents impacting the regolith simulant sample. Since chamber wall collision effects are not expected to depend on the incident charge state of a given incident projectile species for fixed incident energy, the particle-current-normalized sputtered mass spectra for the different incident multiply charged Ar ions compared to that for singly charged Ar will directly reflect the enhancement due to potential sputtering effects. In comparing the particle-current-normalized sputtered mass distributions for incident protons and incident singly charged Ar species, we are not able to eliminate the possibility of wall collision effects due to potentially different reflection coefficients for the investigated sample. Comparison with the SRIM values of [1] and published measurements for H^+ and Ar^+ induced sputtering yields for SiO_2 [15,16] and Al_2O_3 [16], which are major constituents of the JCS-1A AGGL lunar regolith simulant, shows similar differences between the two species as observed in the present investigation, suggesting that wall collision effects are not significantly different for the two incident species at 375 eV/amu. The sputtered particle mass distributions were monitored as function of accumulated sample fluence for selective depletion of species such as oxygen, which is one of the signatures of defect mediated (electronic) sputtering [3]. Such depletion has been inferred from changes in total (i.e. unresolved in mass) sputtering yields [3]. Its explicit measurement would permit determination of the solar wind exposure time at which this depletion could take place in the absence of grain vaporization, gardening and other turn-over effects due to, e.g. micrometeorite impact, which act to reinitialize the lunar surface. Determination of this depletion time scale in relation to the reinitialization time scale is crucial in the assessment of possible potential sputtering effects on the real lunar surface.

3. Results

Fig. 3 shows mass scans in the range 2–24 amu produced by normal incidence impact of 375 eV/amu protons, Ar^+, Ar^{6+}, and Ar^{9+} ions on our lunar regolith simulant target at room temperature, acquired with the QMS in our floating scattering chamber as described in the previous section. The mass scans are normalized by the respective beam particle currents, so that all the spectra are comparable on the same relative scale. The prominent mass 20 peaks evident for the Ar^{q+} beam produced spectra are due to Ar^{2+} ions produced in the QMS ionizer, and represent Ar loading of our scattering chamber vacuum due to the different Ar^{q+} beams. Since no trapping or other accumulation of Ar is expected for our simulant target,

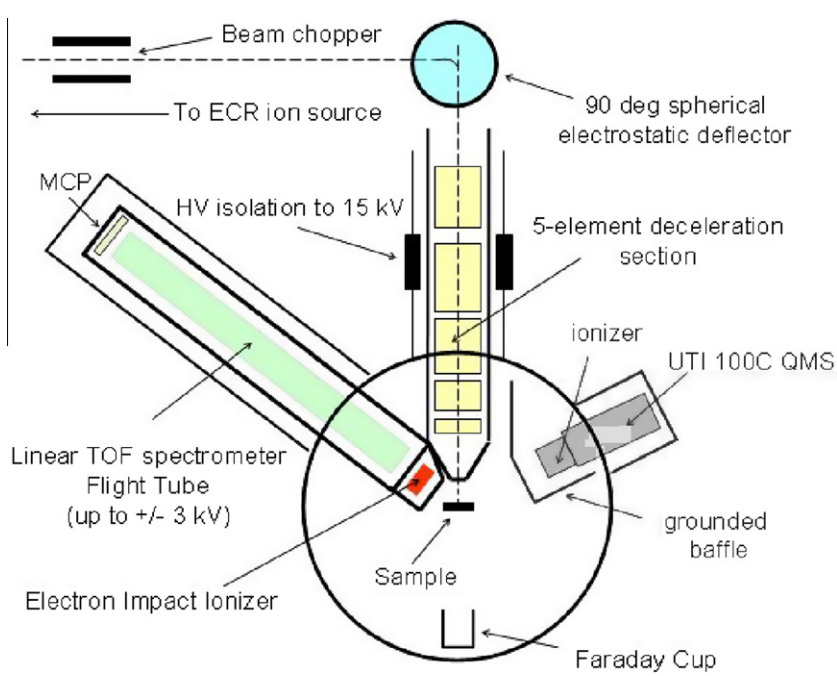

Fig. 2. Schematic of the floating surface scattering chamber used for the sputtering measurements. Not shown is the wire scanner to determine incident beam profiles, and the sputter gun for surface cleaning.

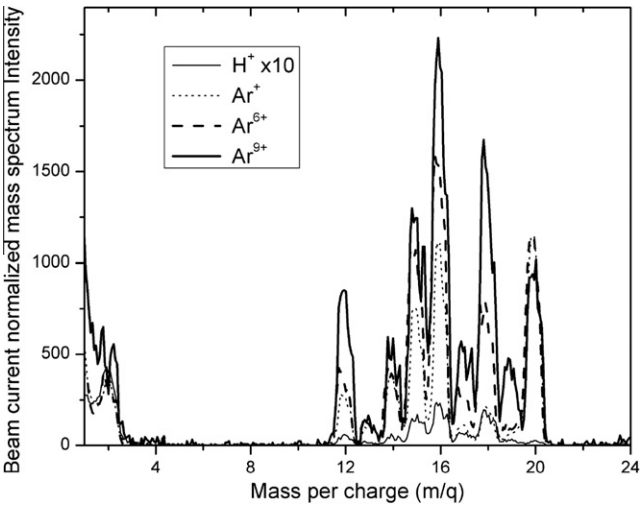

Fig. 3. Mass distribution of sputtered species and beam species reemission in the range 2–24 amu, normalized to the respective beam particle currents for protons, Ar^{+}, Ar^{6+}, and Ar^{9+} incident on room temperature lunar regolith simulant at 375 eV/amu.

the mass 20 peak heights are directly proportional to the particle currents of the various Ar^{q+} beams. The very similar mass 20 peak heights evident in Fig. 3 for the different Ar^{q+} beams confirm and support the validity of our applied current-normalization procedure. To simulate the effect of the H loading of the surface due to the dominant H constituent of the solar wind, prior to each of the Ar beam exposures, the sample was exposed to a high fluence ($\sim 10^{18}/cm^2$) of 375 eV protons. The Ar beam produced spectra were acquired for a range of different accumulated fluences up to 10^{15}–$10^{16}/cm^2$, in an attempt to document a possible fluence dependent decrease in the O related mass peaks, inferred in earlier measurements for metal oxide targets at fluences in excess of 10^{13}–$10^{14}/cm^2$ [3,17,18]. Typical beam fluxes were in the range 10^{14}–$10^{15}/cm^2$ s. We did not observe any fluence dependence in the mass spectra for any of the incident beams. This may mean either that, for our sample, selective O depletion does not occur, or that the critical fluence for O depletion occurs at higher values than the maximum fluences reached in the present measurements due to the increased, fractal like, surface area of the compressed powder in comparison to the polycrystalline surfaces used in Refs. [17–19].

4. Discussion

Focusing for the moment on the mass-16 (O) peaks in the spectra shown in Fig. 3, the difference between the Ar^{+} and H^{+} induced O production is a factor of about 80 at 375 eV/amu. The increased yield for the heavier incident ion is due to the mass dependence of physical sputtering. The observed physical sputtering enhancement is consistent with published measurements of H^{+} and Ar^{+} induced total sputtering yields for Al_2O_3 and SiO_2 [15,16] at this energy, which indicate enhancements in total sputtering yields for those two metal oxide targets of ~80 and ~90, respectively. This gives some confidence that the present technique is able to provide reasonable estimates of relative sputtering yields. The multicharged Ar induced spectra show a clear potential sputtering enhancement in O production over the Ar^{+} induced spectrum, giving a 50% increase for incident Ar^{6+} and a factor of two increase for Ar^{9+}. Similar enhancements are seen for the other major mass peaks in the investigated mass range. For comparison, the measurements of Sporn et al. [19] for Ar^{q+} ions incident on SiO_2 show a factor of ~2.7 greater sputtering yield for Ar^{8+} than for Ar^{+} at 1 keV (i.e. 0.025 keV/amu), their highest investigated energy. The trend established by their lower energy measurements, i.e. a factor of ~4 at 200 eV, and a factor of ~3 at 500 eV, indicates a decreasing enhancement factor with increasing energy, so not inconsistent with our factor of about two observed at 15 keV (375 eV/amu).

The peaks at mass 17, 18, and 19 suggest OH, H_2O and H_3O formation during the high fluence proton exposures prior to each Ar beam run. However, at present we are not able to exclude the possibility that these OH_x peaks originate from wall collisions of target-emitted O atoms prior to entering our baffled QMS. More definitive measurements with a new line-of-sight QMS, less susceptible to wall collision effects, are planned to address the interesting question of H beam induced chemistries, including water formation, that may occur in our lunar regolith simulant sample.

Regarding the SEM morphology and XPS chemical composition analyses for the two different sample preparation methods, a comparison of Figs. 1a and 1b suggests that significant grain crushing had occurred during the pressing process. As a result, the amorphous rim structures for the pressed sample were most likely largely destroyed. In addition to the higher adventitious C concentration measured for the powder sample gently pressed onto C-tape, systematic lowering of some of the metal constituents was observed (Si, Al, Ca, Mg, and Na). Further measurements are needed to assess whether these decreases reflect the composition of intact vs. destroyed rims, or are merely compositional variations of the bulk simulant powder.

5. Summary and conclusions

Preliminary measurements have been presented of relative O sputtering by 375 eV/amu H^{+}, Ar^{+}, Ar^{6+}, and Ar^{9+} ions incident on room temperature JSC-1A AGGL lunar regolith simulant. Compared to the proton induced O yield, O production by incident same-velocity Ar^{+} is increased by a factor of ~80, and an additional factor of two for incident Ar^{9+}. No significant fluence dependences in O production were observed up to the maximum fluences investigated (10^{15}–$10^{16}/cm^2$). The measurements were obtained for a pressed sample which most likely compromised the integrity of the amorphous "rim" melt layer (see Fig. 1a). Since all the interactions of solar wind ions and lunar regolith occur in the rim, and in view of the implications of changes of the rim chemical composition in comparison to that of the bulk, as outlined in [1], the need is underscored for additional measurements with a sample for which the rim structures are intact, e.g. as is shown in Fig. 1b. Such measurements are planned, and will be carried out with a new line-of-sight QMS system presently being installed, which should also provide more definitive insights into the issue of H beam induced chemistries in the metal oxide constituents of lunar regolith. Further insights on this question could be provided by future line-of-sight TOF measurements to search for enhanced H^{+} emission from H beam loaded lunar regolith samples by highly charged ions [20]. Finally, XPS sample analyses after exposures to varying fluence multicharged ion beams are planned to experimentally test the rim compositional changes calculated in [1].

Acknowledgments

This research is supported by the ORNL LDRD program, and the US Department of Energy, Office of Basic Energy Sciences. We thank Dr. Edwin Ethridge of NASA-Marshall Space Flight Center for providing us with the JSC-1A AGGL simulant. PRH was appointed through the ORNL Postdoctoral Research Associates Program administered jointly by Oak Ridge Institute for Science and Education and Oak Ridge National Laboratory.

References

[1] A.F. Barghouty, F.W. Meyer, P.R. Harris, J.H. Adams, these proceedings.
[2] T. Schenkel, A.V. Hamza, A.V. Barnes, D.H. Schneider, Prog. Surf. Sci. 61 (1999) 23–84.
[3] F. Aumayr, H.P. Winter, Phil. Trans. R. Soc. Lond. A 362 (2004) 77–102.
[4] G.H. Heiken, D.T. Vaniman, B.M. French, Lunar Source Book: A User's Guide to the Moon, Cambridge Univ. Press (Cambridge, England), 1991, CD version by Lunar and Planetary Institute, 3600 Bay Area boulevard, Houston, TX 77058-1113, 2005 (Chapter 7).
[5] R. von Steiger, N.A. Schwadron, L.A. Fisk, J. Geiss, G. Gloecker, S. Hefti, B. Wilken, R.F. Wimmer-Schweingruber, T.H. Zurbuchen, J. Geophys. Res. 105 (2000) 217–227.
[6] S.J. Bame, J.R. Asbridge, W.C. Feldman, M.D. Montgomery, P.D. Kearney, Solar Phys. 43 (1975) 463–473.
[7] http://www.orbitec.com/.
[8] F.W. Meyer, M.E. Bannister, D. Dowling, J.W. Hale, C.C. Havener, J.W. Johnson, R.C. Juras, H.F. Krause, A.J. Mendez, J. Sinclair, A. Tatum, C.R. Vane, E. Bahati Musafiri, M. Fogle, R. Rejoub, L.I. Vergera, Nucl. Instr. and Meth. Phys. Res. B 242 (2006) 71–79.
[9] F.W. Meyer, H. Zhang, M.J. Lance, H.F. Krause, Vacuum 82 (2008) 880–894.
[10] I.G. Hughes, J. Burgdörfer, L. Folkerts, C.C. Havener, S.H. Overbury, M.T. Robinson, D.M. Zehner, P.A. Zeijlmans van Emmichoven, F.W. Meyer, Phys. Rev. Lett. 71 (1993) 291–294.
[11] V.A. Morozov, F.W. Meyer, Phys. Rev. Lett. 86 (2001) 736–739.
[12] V.A. Morozov, F.W. Meyer, P. Roncin, Phys. Scripta T80A (1999) 69–76.
[13] F.W. Meyer, M.E. Bannister, J.W. Hale, C.C. Havener, H.F. Krause, C.R. Vane, S. Deng, I.N. Draganić, P.R. Harris, in: Proc. of the XIXth International Workshop on ECR Ion Sources, Grenoble, France, August 23–26, 2010, to appear http://accelconf.web.cern.ch/AccelConf/ecris10/proceedings.pdf/MOCOBK04.
[14] L.I. Vergara, F.W. Meyer, H.F. Krause, J. Nucl. Mater. 347 (2005) 118.
[15] T. Nenadović, B. Perraillon, Ž. Bogdanovich, Z. Djordjević, M. Milić, Nucl. Instr. and Meth. Phys. Res. B 48 (1990) 538.
[16] J. Roth, J. Bohdansky, W. Ottenberger, Max-Planck IPP Report 9/26, May 1979.
[17] G. Hayderer, S. Cernusca, V. Hoffmann, D. Niemann, N. Stolterfoht, M. Schmid, P. Varga, H.P. Winter, F. Aumayr, Nucl. Instr. and Meth. Phys. Res. B 182 (2001) 143.
[18] G. Hayderer, S. Cernusca, M. Schmid, P. Varga, H.P. Winter, F. Aumayr, D. Niemann, V. Hoffmann, N. Stolterfoht, C. Lemell, L. Wirtz, J. Burgdörfer, Phys. Rev. Lett. 86 (2001) 3530.
[19] M. Sporn, G. Libiseller, T. Neidhart, M. Schmid, F. Aumayr, H.P. Winter, P. Varga, M. Grether, N. Stolterfoht, Phys. Rev. Lett. 79 (1997) 945.
[20] M. Kakutani, Y. Azuma, K. Komaki, K. Kuroki, Nucl. Instr. and Meth. Phys. Res. B 96 (1995) 541–544.